4-2010

Adaptive Passive Fathometer Processing

Martin Siderius
Portland State University, siderius@pdx.edu

Heechun Song
Marine Physical Laboratory

Peter Gerstoft
Marine Physical Laboratory

William S. Hodgkiss
Marine Physical Laboratory

Paul Hursky
HLS Research Inc.

See next page for additional authors

Citation Details

Siderius, M., Song, H., Gerstoft, P., Hodgkiss, W., Hursky, P., & Harrison, C. (2010). Adaptive passive fathometer processing. The Journal of The Acoustical Society of America, 127(4), 2193-2200.

Adaptive passive fathometer processing

Martin Siderius
Department of Electrical and Computer Engineering, Portland State University, Portland, Oregon 97201

Heechun Song, Peter Gerstoft, and William S. Hodgkiss
Marine Physical Laboratory, Scripps Institution of Oceanography, La Jolla, California 92093-0238

Paul Hursky
HLS Research Inc., 3366 North Torrey Pines Court, Suite 310, La Jolla, California 92037

Chris Harrison
NATO Undersea Research Centre, Viale San Bartolomeo, 400, 19126 La Spezia, Italy

(Received 13 October 2009; revised 7 January 2010; accepted 8 January 2010)

Recently, a technique has been developed to image seabed layers using the ocean ambient noise field as the sound source. This so called passive fathometer technique exploits the naturally occurring acoustic sounds generated on the sea-surface, primarily from breaking waves. The method is based on the cross-correlation of noise from the ocean surface with its echo from the seabed, which recovers travel times to significant seabed reflectors. To limit averaging time and make this practical, beamforming is used with a vertical array of hydrophones to reduce interference from horizontally propagating noise. The initial development used conventional beamforming, but significant improvements have been realized using adaptive techniques. In this paper, adaptive methods for this process are described and applied to several data sets to demonstrate improvements possible as compared to conventional processing.
 [DOI: 10.1121/1.3303985]

PACS number(s): 43.30.Wi, 43.30.Pc, 43.30.Gv, 43.30.Nb [AIT] Pages: 2193–2200

I. INTRODUCTION

In sonar terminology, passive systems listen only while active systems transmit a signal and then receive and process the echoes. The echoes contain information about objects such as their distance and size. This is the basis for echolocation used by bats to hunt for insects in the dark. In the ocean, active sonars use sound projectors to transmit a signal. Recent work has shown that acoustic noise such as that from breaking waves can be used as a coherent sound source for "active" sonar processing.[1] Using noise this way, the sonar itself is passive but active sonar processing methods can be exploited. Previous noise processing methods have used noise intensity to estimate seabed layering[2,3] or seabed geoacoustic properties;[4,5] however, coherent noise processing differs since absolute depths of the seabed and sub-bottom layers are recovered. This coherent technique has been referred to as passive fathometer processing.[1] Since that initial passive fathometer work, theoretical expressions to show the dependency on factors such as averaging time, beam size, and the effects of measurements taken over a rough seabed were developed[6] and effects of sea-surface conditions on passive fathometry have been studied.[7]

A mathematical description of the processing in time and frequency was given in Ref. 8 where the adaptive passive fathometer was introduced. The sign of the adaptive reflection sequence has also been discussed.[9,10] The purpose of this article is to describe how adaptive processing can be applied to passive fathometer techniques and to demonstrate the advantages with several data sets.

Noise based sonar has several practical advantages: (1) There has been significant objection in recent years to man-made sounds in the ocean from either sound projectors or explosive sources. The effect of these sounds is difficult to quantify but in extreme cases has been implicated in marine mammals stranding themselves.[11] In less extreme situations, the sounds may cause behavior changes in marine life and this might be significant especially when this occurs in protected areas or around endangered species. (2) Using noise instead of a projector can greatly simplify the measurements. This is especially true when separations between the sound source and receiver are needed (e.g., to obtain different reflection angles off the seabed). Further, noise is usually very broadband and obtaining a sound source with as much bandwidth can be challenging. (3) Using ambient noise, and thus not having to expend battery power using an active transmitter, is especially attractive in autonomous systems, since this will significantly extend their missions, which in this instance will increase the area being mapped out.

The basis for the passive fathometer is the cross-correlation between the surface noise generated by breaking waves, and the echo return from the seabed. Except at lower frequencies dominated by shipping, breaking waves commonly are the predominant source of ambient noise. It is important to note that the passive fathometer processing is coherent, which is essential to preserve the travel times to the seabed and layers beneath. Coherent processing of noise signals dates back several years. Rickett and Claerbout[12] investigated this for seismic signals, and Weaver and Lobkis[13,14] explored applications in ultrasonics. For ocean acoustics, a

coherent arrival structure was obtained using horizontally separated noise measurements.[15–17] A theoretical framework for recovering Green's functions between point receptions of ocean noise has also been developed.[18–20] One of the differences between the passive fathometer applications and previous work is the use of beamforming to focus the received energy on the useful noise and reduce interference from unwanted noise sources. This has the effect of improving the estimates for seabed layering while reducing the needed averaging time.

This paper is organized as follows: Section II describes the processing methods. The conventional beamforming approach is described here for completeness, and is presented in a slightly more compact way than previously.[1] In addition, the adaptive methods are described that includes a description of the white noise gain constraint beamformer. Section III gives several examples with different hydrophone arrays, locations, and for both stationary and moving arrays.

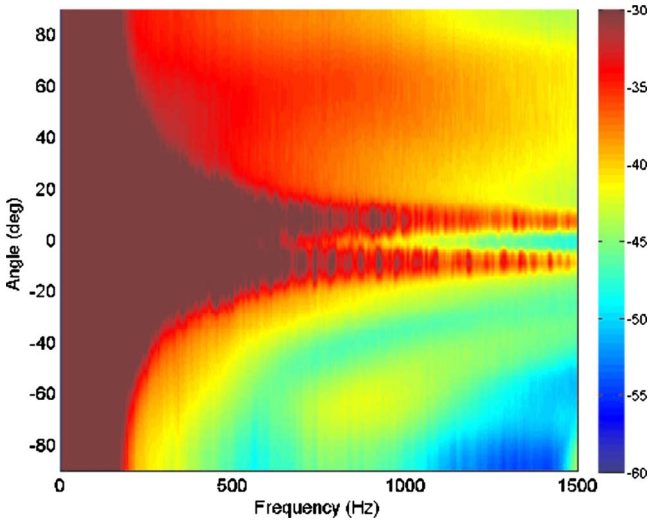

FIG. 1. (Color online) Conventional beamforming applied to 3 min of ocean noise data from the MAPEX2000bis experiment.

II. PROCESSING METHODS

The cross-correlation between the noise from the ocean surface and its echo from the seabed produces a time trace with peaks representing the water-sediment interface as well as sub-bottom layers. One of the key differences between typical noise correlation and the passive fathometer method is the use of a vertical hydrophone array. The array is used to emphasize the noise directly above rather than from horizontal directions. The details of the conventional passive fathometer are described in Sec. II A, and the extension for adaptive processing follows in Sec. II B.

A. Conventional passive fathometer

In the original formulation, conventional beamforming was used and a brief summary is given here. The hydrophone data for each channel at angular frequency ω are written as a column vector $\mathbf{p}=[p_1,p_2,\ldots,p_M]$ for the M hydrophones. Each entry is determined through a Fourier transform [implemented using the fast Fourier transform (FFT)] of an ambient noise time series measured on each channel, $p_m(\omega)=\mathcal{F}\{p_m(t)\}$. The number of sample points in the FFT processing will be referred to as the snapshot size (the snapshot size may equivalently be expressed in seconds by dividing the number of sample points by the sampling frequency).

With conventional beamforming, the weight for the mth hydrophone steered at angle θ for plane waves arriving at grazing angle θ between the hydrophones separated by distance d is written as

$$w_m = e^{-imkd\sin\theta}. \tag{1}$$

The array is referenced to the shallowest hydrophone, which is element $m=0$. The wavenumber is $k=\omega/c$ and c is the sound speed in the water (around 1500 m/s).

Writing the steering weights as a column vector, $\mathbf{w}=[w_0,w_1,\ldots,w_{M-1}]$, the beam $b(\theta)$ is written as

$$b(\theta)=\mathbf{w}^{\dagger}\mathbf{p}, \tag{2}$$

where † represents the conjugate transpose operation. The conventional instantaneous beam power for a given direction θ is computed by the following:

$$B(\theta)=\mathbf{w}^{\dagger}\mathbf{p}(\mathbf{w}^{\dagger}\mathbf{p})^{\dagger}=\mathbf{w}^{\dagger}\mathbf{p}\mathbf{p}^{\dagger}\mathbf{w}=\mathbf{w}^{\dagger}\mathbf{K}\mathbf{w}, \tag{3}$$

where the single snapshot cross-spectral density matrix (CSDM) $\mathbf{K}$ is identified as $\mathbf{p}\mathbf{p}^{\dagger}$. Forming the CSDM allows for multiple snapshots to be averaged before beamforming.

An example of conventional beamforming ocean noise can be illustrated using data from the MAPEX2000bis experiment[5,21] (see Fig. 1). These data were collected by the NATO Undersea Research Centre in the Strait of Sicily between Italy and Malta in November 2000 and analyzed in Refs. 2, 8, and 21. The array had 64 hydrophones of different separations and, here, the 0.5 m equally spaced 32 hydrophones of the array were used for analysis. The array was positioned in about 130 m water depth and moored to the bottom. 3 min of data were averaged to form the CSDM used for beamforming. Figure 1 shows the beamformed output normalized for a maximum of 0 dB (note that the color scaling is from −60 to −30 dB so that all values greater than −30 dB appear in color as the −30 dB value). The positive angles correspond to the beams steered toward the surface (up-looking beams), which capture signals traveling downward from the surface. The negative angles are beams steered down toward the seabed (down-looking beams) and capture signals traveling upward from the seabed. In Fig. 1, the higher intensity noise is evident on the up-looking beams since the down-looking beams see the surface through a seabed reflection and therefore experience losses. Also note the high intensity noise coming from near horizontal. These data consist of a variety of noise sources including breaking waves and distant shipping.

For passive fathometer processing, the interest is in correlating the up-looking beam with the down-looking beam rather than forming the beam power at each grazing angle. To steer an up-looking beam directly upward toward the sur-

face, $\theta=+90°$, and to steer directly toward the seabed, $\theta=-90°$. The steering weights are $w_m=e^{\mp(imkd)}$ and the up-looking weight will be denoted $\mathbf{w}_+$ and the down-looking as $\mathbf{w}_-$. Therefore,

$$b_{\mathrm{up}}=\mathbf{w}_+^{\dagger}\mathbf{p}, \tag{4}$$

and the downward beam

$$b_{\mathrm{dn}}=\mathbf{w}_-^{\dagger}\mathbf{p}. \tag{5}$$

Expressed in the frequency domain, the correlation of these two beams is

$$C=(\mathbf{w}_-^{\dagger}\mathbf{p})(\mathbf{w}_+^{\dagger}\mathbf{p})^{\dagger}=\mathbf{w}_-^{\dagger}\mathbf{p}\mathbf{p}^{\dagger}\mathbf{w}_+=\mathbf{w}_-^{\dagger}\mathbf{K}\mathbf{w}_+. \tag{6}$$

But, for conventional processing, the down-looking beam is just the conjugate of the up-looking beam $\mathbf{w}_-=\mathbf{w}_+^*$. The conventional beamforming correlation then can be written simply using $\mathbf{w}=\mathbf{w}_-$ as follows:

$$C=\mathbf{w}^{\dagger}\mathbf{K}\mathbf{w}^*. \tag{7}$$

The conventional passive fathometer in Eq. (7) differs only from the conventional beamformer output given by Eq. (3) in that the $\mathbf{w}$ to right is conjugated. As a result, B is positive real and C is a complex number. The corresponding phase of C contains the information on the reflection arrival times. As with conventional beamforming, the CSDM given in Eq. (7) can be formed over as many snapshots of data $\mathbf{p}$ as needed to obtain the desired averaging. Averaging time may vary depending on factors such as array motion, noise level, and number of elements in the array.

B. Adaptive passive fathometer

As evident in Fig. 1, there is significant noise intensity at grazing angles near horizontal. This high intensity noise away from the +90° and −90° directions (i.e., away from endfire) degrade the passive fathometer output due to leakage through sidelobes. Sidelobe leakage is a common problem in beamforming and one of the mitigation strategies is to use adaptive methods such as minimum variance distortionless response (MVDR).[22,23] To adaptively beamform using MVDR, the steering weights $\tilde{\mathbf{w}}$ are computed according to

$$\tilde{\mathbf{w}}=\frac{\mathbf{K}^{-1}\mathbf{w}}{\mathbf{w}^{\dagger}\mathbf{K}^{-1}\mathbf{w}}. \tag{8}$$

Using Eq. (7) and continuing to assume $\tilde{\mathbf{w}}_-=\tilde{\mathbf{w}}_+^*$, the MVDR correlation at frequency ω is

$$C_A=\tilde{\mathbf{w}}^{\dagger}\mathbf{K}\tilde{\mathbf{w}}^*. \tag{9}$$

Note that for the typical application of MVDR beamforming (as opposed to cross-correlating beams), the beamformer output can be written as was done in Eq. (3) but with adaptive weights

$$B_A(\theta)=\tilde{\mathbf{w}}^{\dagger}\mathbf{K}\tilde{\mathbf{w}}. \tag{10}$$

And, using Eq. (8), the beamformer output reduces to a much simpler expression that uses the conventional weights

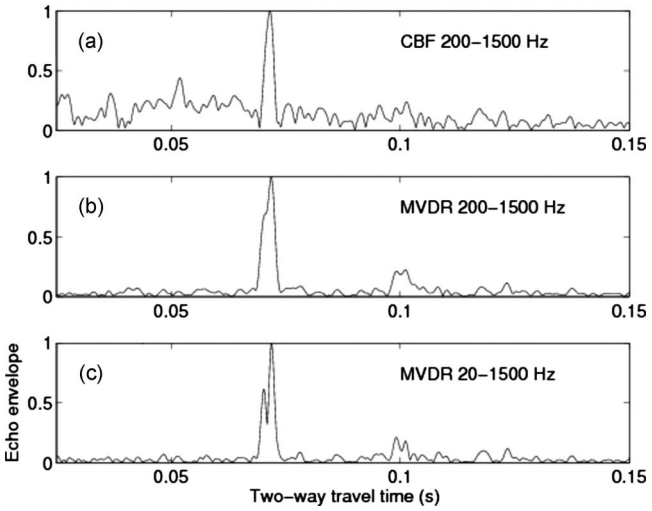

FIG. 2. Example of conventional beamforming (a) and adaptive (MVDR) beamforming (b) on the same cross-spectral density matrix of data. The envelope of $c(t)$ is shown using a 200–1500 Hz band. Panel (c) shows MVDR results in the 20–1500 Hz band.

$$B_A(\theta)=\left[\frac{\mathbf{K}^{-1}\mathbf{w}}{\mathbf{w}^{\dagger}\mathbf{K}^{-1}\mathbf{w}}\right]^{\dagger}\mathbf{K}\left[\frac{\mathbf{K}^{-1}\mathbf{w}}{\mathbf{w}^{\dagger}\mathbf{K}^{-1}\mathbf{w}}\right]=(\mathbf{w}^{\dagger}\mathbf{K}^{-1}\mathbf{w})^{-1}. \tag{11}$$

MVDR is sometimes implemented with this expression since it is less computationally involved than Eqs. (8) and (10).

For adaptive processing, the weights for up- and down-looking beams are not necessarily conjugates of each other (i.e., $\tilde{\mathbf{w}}_-\neq\tilde{\mathbf{w}}_+^*$), and the correct expression for the correlation is

$$C_A=\tilde{\mathbf{w}}_-^{\dagger}\mathbf{K}\tilde{\mathbf{w}}_+. \tag{12}$$

For implementation, we derive the up- and down-looking beam adaptive weights separately using Eq. (8) and then compute the correlation using Eq. (12). The time-series passive fathometer response is simply the inverse Fourier transform of C or $c(t)=\mathcal{F}^{-1}\{C(\omega)\}$ (or the inverse Fourier transform of C_A). For a one-dimensional (1D) medium with a single point source Green's function is proportional to the noise cross-correlation $c(t)$.[8] This model resembles the main wave propagation for the fathometer and thus the reflection response is proportional to $c(t)$. It should be mentioned that the adaptive processing introduces a negative sign on the main reflections although this is not important here where only the envelope of $c(t)$ is considered. Recently the sign anomaly was explained mathematically under simplifying assumptions.[9]

An example of the difference between conventional and MVDR adaptive beamforming is shown in Fig. 2. Both results use the same CSDM averaged over 3 min (same CSDM as used in Fig. 1). The envelope of the time domain expression $c(t)$ is shown in panel (a) for conventional beamforming in the band 200–1500 Hz processed using Eq. (6). Panel (b) shows the MVDR results in the same band using Eq. (9). Panel (c) of Fig. 2 shows MVDR over a larger bandwidth of 20–1500 Hz. The MVDR better rejects the horizontal noise (see Sec. III B) and therefore it is possible to include lower frequencies, which penetrate farther into the seabed, and with the increased bandwidth better time resolution is possible.

C. White noise gain constraint

Since MVDR processing involves inverting the CSDM, problems can occur when the matrix is less than full rank. To stabilize the inversion, the MVDR weights are recast with diagonal loading

$$\tilde{\mathbf{w}} = \frac{[\mathbf{K} + \epsilon\mathbf{I}]^{-1}\mathbf{w}}{\mathbf{w}^{\dagger}[\mathbf{K} + \epsilon\mathbf{I}]^{-1}\mathbf{w}}, \tag{13}$$

where $\mathbf{I}$ is the identity matrix and the ϵ parameter is the adjustable diagonal loading strength. The diagonal loading is equivalent to adding white noise with its power depending on the strength parameter ϵ.[24]

In cases considered here, the array is either stationary or slowly drifting, and there is no snapshot deficiency. However, the MVDR processor is also known to be sensitive to mismatch. For example, this mismatch can come in the form of environmental factors (such as non-plane-wave propagation) or the actual array shape being different from the assumed shape. The white noise gain constraint beamformer[25] adjusts ϵ for each angle to provide robustness to the adaptive processor, which is constrained by the value selected for the white noise gain constraint δ^2 such that

$$\delta^2 \leq G_w \leq M, \tag{14}$$

where the white noise gain G_w is defined by

$$G_w = |\tilde{\mathbf{w}}^{\dagger}\tilde{\mathbf{w}}|^{-1}, \tag{15}$$

and M is the number of hydrophones. The white noise gain constraint beamformer can be tuned to be pure MVDR ($\epsilon=0$), pure conventional ($\epsilon=\infty$), or somewhere in between, according to the value selected for δ^2. Algorithmically, for any given angle, the diagonal loading ϵ is increased until constraint equation (14) is satisfied. Unfortunately, the relationship between ϵ and δ^2 is not simple except that the upper limit of $\delta^2=M$ corresponds to pure conventional ($\epsilon=\infty$). In typical sonar processing (e.g., detecting weak targets), a normalized δ^2, defined by $\mathrm{WNC}=10\log(\delta^2/M)$ dB, is set to -2 or -3 dB.[24] However, for passive fathometer processing, the WNC value is set to -10 dB, as will be presented in Sec. III.

III. RESULTS

The previous example for the MAPEX2000bis experiment shown in Fig. 2 illustrated the benefits of adaptive over conventional beamforming. The adaptive approach has better time resolution, better "signal-to-noise" ratio, and shows sub-bottom layers that are not evident in the conventional results. But, are these resolved layers in the adaptive processing real? In the next sections different arrays are used along with seismic profile data to build the case for the adaptive results being correct and a significant improvement over the conventional processing. In Sec. III A, the MAPEX2000bis example along with an additional data set are presented. In each case a different array is used but both are stationary (i.e., moored). The fixed geometry simplifies the analysis and also demonstrates performance improvements using adaptive methods in different frequency bands and with different arrays. To map a seabed, the array will be moving and two cases using drifting arrays are given in Secs. III B and III C.

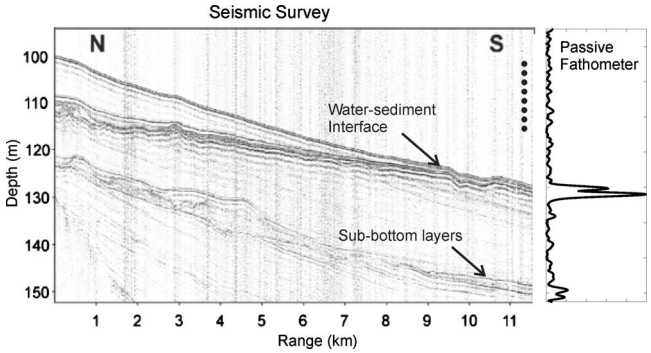

FIG. 3. Left side shows the sub-bottom profile for the MAPEX2000bis site (sub-bottom profile from Ref. 26) along with the adaptive passive fathometer result shown on the right. The approximate position of the vertical array is indicated by the vertical dots in the sub-bottom profile.

A. Adaptive vs conventional processing with fixed arrays

Figure 3 shows the passive fathometer time trace (far right of figure) along with a corresponding seismic profile taken in the same location. The fixed array was located at the south end of the seismic track; the approximate array location is indicated in the figure near range 11 km and is denoted using black vertical dots. The passive fathometer time trace gives an indication of some interfering layers near the water-sediment interface, which is consistent with the joining of two layers in the seismic profile. Also, the passive fathometer shows two sub-bottom layers approximately 20 m below the water-sediment interface. Recall that in Fig. 2 the conventional processing did not resolve layers near the water-sediment interface and the deeper layers are not identifiable.

The next data set considered is from Dabob Bay in Washington; see Fig. 4. This is a well protected area with the middle of the Bay approximately 180–200 m deep. The array

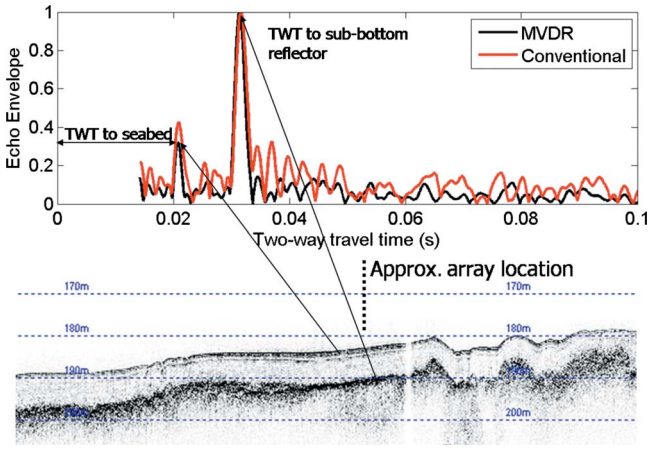

FIG. 4. (Color online) Adaptive passive fathometer result for Dabob Bay experiment. Top panel shows the passive fathometer response (conventional and MVDR adaptive processing). Lower panel shows the sub-bottom profile and the approximate array location. Note the correspondence between the layers in the two plots as well as the improvement in the response using MVDR.

used here had 16 hydrophones at 0.5 m spacing with first phone at 15 m off the seafloor. The frequency band used for the MVDR processing was 50–1500 Hz. After the experiment a sub-bottom profile was taken using the Knudsen 320B system on the R/V New Horizon. The water depth was about 185 m. The short two way travel time (TWT) from the array to the seabed (about 0.02 s) is because the array was moored close to the seabed (about 7.5 m from the bottom hydrophone to the seabed). The passive fathometer return shows a relatively weak arrival at the water-seabed interface at about 0.02 s TWT with a much stronger return at around 0.03 s. This stronger second return suggests a higher impedance contrast for the second interface. This also is suggested in the sub-bottom profile. For comparison, the conventional processing result is also superimposed in Fig. 4, exhibiting higher noise levels especially just past the second peak (0.03 s).

B. Adaptive vs conventional processing with drifting arrays: Boundary 2003

The next experimental example is from a drifting array during the NURC's Boundary 2003 experiment. These experiments were originally set up to test out a different technique (spectral factorization) for investigating layer echoes[2,3] and also bottom reflection properties.[5] The first part of this track was processed previously using the conventional passive fathometer approach.[1] The drifting array has 32 hydrophones spaced at 0.18 m (design frequency of 4.2 kHz). The depth of the reference hydrophone was approximately 73.5 m. The wind varied during the experiment but was, on average, about 15 kn. In this case, the moving array limits the number of snapshots that can be taken per time trace and, here, snapshots were averaged over 90 s to form the CSDM. The adaptive processing parameters for these data were as follows: frequency band 50–4000 Hz, snapshot size T_{snap} = 1.4 s, and total averaging time T_{ave} = 90 s. For the conventional processing the same parameters were used. However, the frequency band was reduced to 200–4000 Hz because of significant shipping noise below 200 Hz that cannot be suppressed using the conventional approach.

Results for the Boundary 2003 track using conventional passive fathometer processing are shown in Fig. 5(a). The record number corresponds to a passive fathometer time trace with 90 s of noise averaging time. Therefore each record number (horizontal axis) also equates to range as the array drifted over time. The vertical axis is depth in meters converted from the two way travel times using sound speed of 1500 m/s. Passive MVDR fathometer results are shown in Fig. 5(b). Comparing the conventional processing results [Fig. 5(a)] and adaptive processing [Fig. 5(b)], there are several sub-bottom reflectors that agree with each other. However, the overall image for the conventional processing is less clear than for the adaptive processing. After the drifting array was recovered, a Uniboom (active sonar with towed array) system was used to measure the sub-bottom properties along the same track as the array drifted.[3] It was only possible to approximately capture the array drift track in the survey and the results are shown in Fig. 5(c). In Fig. 5(c) the horizontal axis is the ping number that equates to range since

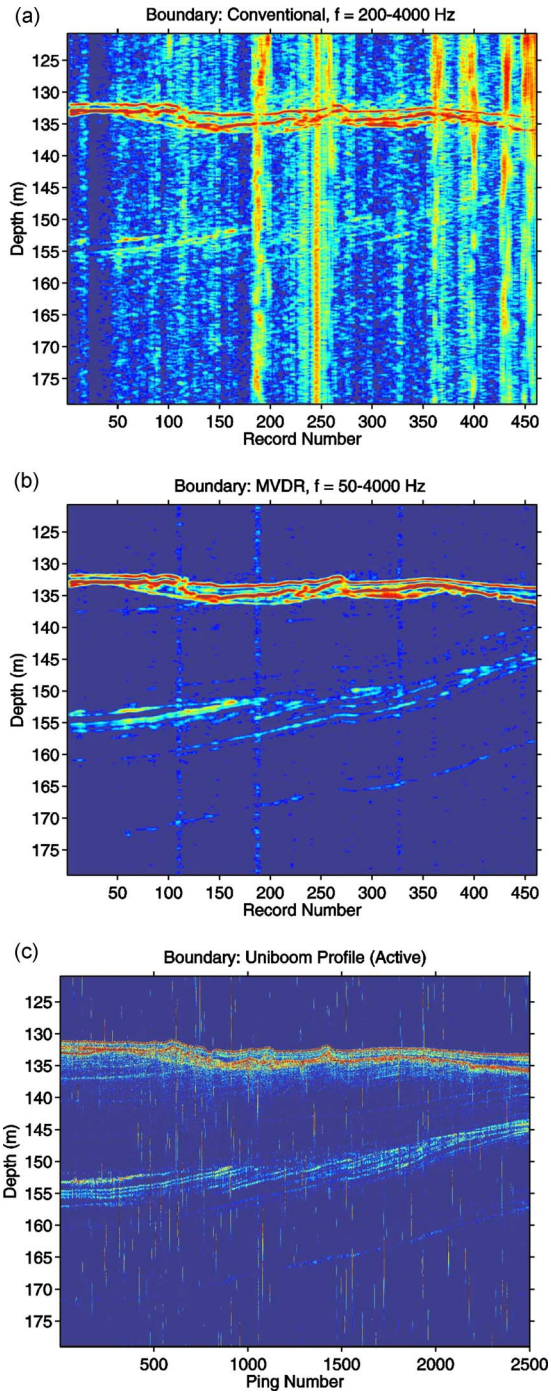

FIG. 5. (Color online) (a) Conventional (200–4000 Hz) and (b) MVDR (50–4000 Hz) passive fathometer results for Boundary 2003 drifting array data. Horizontal axis is the record number that corresponds to range as the array drifted (20 dB dynamic color scale). Panel (c) shows the results from data collected using a Uniboom active seismic system along approximately the same track as the array drift. Ping number on the horizontal axis in (c) corresponds to range along the track (20 dB dynamic color scale).

each ping corresponds to individual transmissions from the Uniboom system as it was towed over the track. Although unlikely that the exact same track was measured with the passive fathometer and the seismic survey, there are several features in the sub-bottom that agree with both the conventional and adaptive results. However, the adaptive passive fathometer results [in Fig. 5(b)] produces an image that is

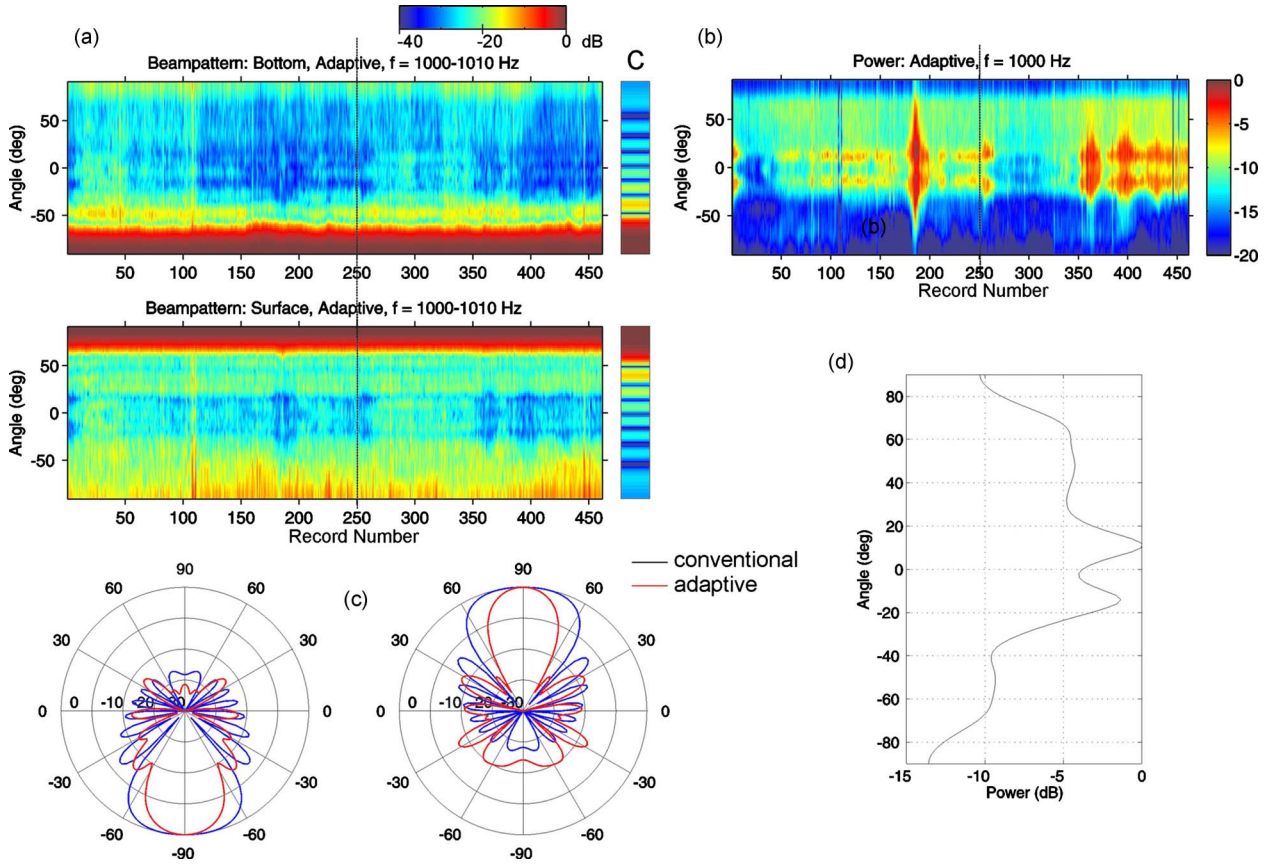

FIG. 6. (Color online) Data from Boundary 2003 in the 1000–1010 Hz band. (a) Down-looking (top panel) and up-looking (bottom panel) beampatterns for the adaptive processing as a function of record number as the array drifts. Conventional beampatterns are constant and are shown as the small vertical bars on the right (labeled C). (b) Beam power output for adaptive processing. As in Fig. 1, the high intensity noise is observed on the up-looking beams. There is strong horizontal energy, which is likely due to distant shipping to be suppressed. (c) Adaptive and conventional polar beampatterns for the down-and up-looking beams used in the passive fathometer for record number 250. (d) A sample slice of the beam power is shown for record number 250.

much more similar to the Uniboom image [in Fig. 5(c)] than does the conventional processing image [in Fig. 5(a)].

This Boundary 2003 data are further analyzed to understand the improvements provided using adaptive processing. In Fig. 6, a beampattern analysis is shown for the 1000–1010 Hz band. In Fig. 6(a), the beampatterns are shown for the adaptive processing as a function of record number as the array drifts. The horizontal axis is the record number that corresponds to range as the array drifts, and the vertical axis is the grazing angle. The top panel in Fig. 6(a) is the down-looking beampattern and the bottom panel is up-looking beampattern, which is quite distinct from the top panel. Recall that only directly up and down steering directions ($\theta = \pm 90°$) are used. Note the regions near horizontal grazing angle in both panels of Fig. 6(a) that are 30–40 dB down where the adaptive processor tries to null the beamform response. In addition, the top panel in Fig. 6(a) suppresses the high intensity beams above horizontal (traveling downward). Anything not coming from straight up or straight down is treated as interference so improvement is achieved by suppressing the interference. Shown in Fig. 6(a) on the far right (small vertical bars) is the conventional beampatterns for comparison. Contrary to adaptive processing where the beampatterns change with time the conventional beampatterns is fixed so only a single plot is needed. Note that the sinc-like pattern for conventional beamforming has much less suppression of the interferers near horizontal.

In Fig. 6(b) the beam power output for adaptive processing is shown along the track as the array drifts. This plot shows the actual beamformed power for all angles (not just the straight up- and down-looking beams). As in Fig. 1, the high intensity noise is observed on the up-looking beams. There also is strong horizontal energy, which is likely due to distant shipping. Not surprisingly, the adaptive beampatterns in Fig. 6(a) show deep nulls around the horizontal. In particular, the event near record number 180 shows a strong interferer, which is being effectively suppressed in Fig. 6(a).

In Fig. 6(c), the adaptive and conventional beampatterns are shown in polar coordinates for the up- and down-looking beams used in the passive fathometer. The conventional beampatterns do not change over time as the data change; however, the adaptive beampatterns are modified depending on the data. Shown in Fig. 6(c) are the adaptive beampatterns for record number 250 along with the conventional beampatterns. The adaptive beampatterns display a sidelobe structure that is quite different from the conventional ones. In particular, note the narrower beams in the $\pm 90°$ directions shown. Also note the differences in the sidelobe structure where the adaptive beams are adjusting to noise coming from direc-

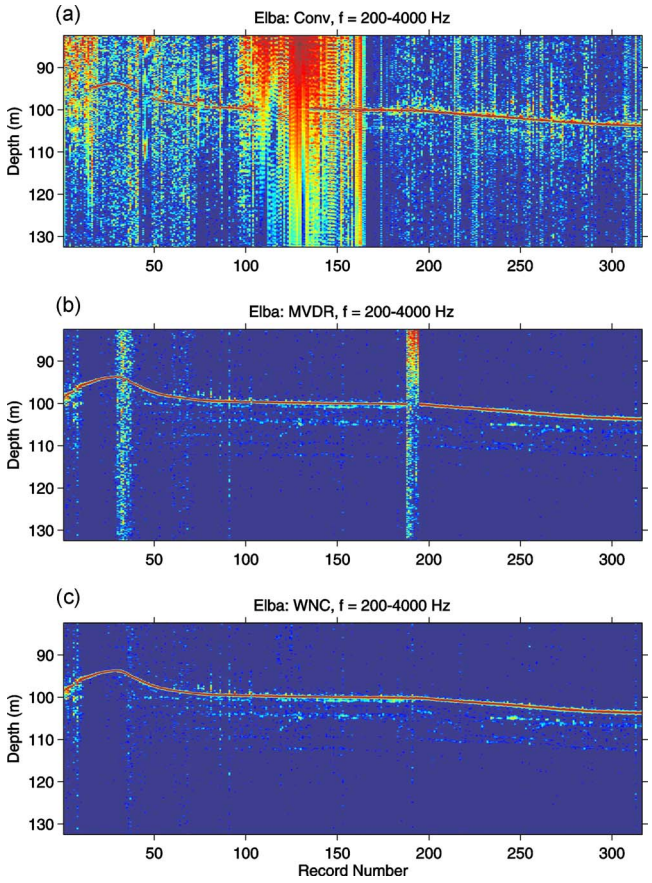

FIG. 7. (Color online) Passive fathometer results from Elba drift: (a) Conventional beamforming, (b) MVDR, and (c) white noise gain constraint beamformer with WNC=−10 dB (20 dB dynamic color scale).

tions other than ±90°. Similarly in Fig. 6(d), a sample slice of the beam power shown in Fig. 6(b) is shown for record number 250.

C. Adaptive vs conventional processing with drifting arrays: Elba

The ElbaEx data were collected between the islands of Elba and Capraia in the Mediterranean Sea in October 2003. The same array as for Boundary 2003 was used with the depth of the reference hydrophone at approximately 73.5 m. Processing parameters used for the Elba data were similar to those for the Boundary data. The frequency band was 200–4000 Hz, snapshot size T_{snap}=0.34 s, and total averaging time T_{ave}=44 s (i.e., the record length). Unfortunately, there were no corresponding seismic data for this drift event. However, it is instructive to compare the conventional and adaptive outputs since the continuity of data along the track provides some measure of the quality of the two results. Shown in Fig. 7 are the results from all three processing types discussed: (a) shows the conventional beamforming passive fathometer, (b) is the straight MVDR, and (c) uses the white noise gain constraint beamformer with WNC=−10 dB. There are regions in (a) that are significantly contaminated in the response and these may be due to local interference effects. While the MVDR (b) is much improved over the conventional approach (a), there still are regions of data contamination. The best results are achieved from the white noise gain constraint beamformer, Fig. 7(c).

IV. CONCLUSION

The passive fathometer processing is a recently developed technique to extract bathymetry and seabed layering information using measurements of ocean ambient noise. This method originally used conventional processing, and the extension to adaptive processing is presented here along with results from several experiments. These experiments used different arrays, and both moored and drifting arrays were used. In all cases, the adaptive results show significant improvements compared to the original conventional results. Adaptive methods allow a larger bandwidth to be included, which gives better time resolution. Further, adaptive methods suppress the horizontal sound that interferes with the surface noise, and this allows weaker sub-bottom layers to be better resolved as compared with conventional processing.

ACKNOWLEDGMENTS

We would like to gratefully acknowledge support for this research by the Office of Naval Research Ocean Acoustics Program. We also would also like to acknowledge the NURC for providing the MAPEX2000bis, Boundary 2003, and ElbaEx data. We would like to thank Peter Nielsen, Mark Stevenson, Finn Jensen, Charles Holland, and Michael Porter for their collaboration on these experiments and data sets, and Keyko McDonald and Brian Granger from SPAWAR for providing the Dabob Bay data.

[1]M. Siderius, C. H. Harrison, and M. B. Porter, "A passive fathometer technique for imaging seabed layering using ambient noise," J. Acoust. Soc. Am. **120**, 1315–1323 (2006).
[2]C. H. Harrison, "Sub-bottom profiling using ocean ambient noise," J. Acoust. Soc. Am. **115**, 1505–1515 (2004).
[3]C. H. Harrison, "Performance and limitations of spectral factorization for ambient noise sub-bottom profiling," J. Acoust. Soc. Am. **118**, 2913–2923 (2005).
[4]M. J. Buckingham and S. A. S. Jones, "A new shallow-ocean technique for determining the critical angle of the seabed from the vertical directionality of the ambient noise in the water column," J. Acoust. Soc. Am. **81**, 938–946 (1987).
[5]C. H. Harrison and D. G. Simons, "Geoacoustic inversion of ambient noise: A simple method," J. Acoust. Soc. Am. **112**, 1377–1389 (2002).
[6]C. H. Harrison and M. Siderius, "Bottom profiling by correlating beam-steered noise sequences," J. Acoust. Soc. Am. **123**, 1282–1296 (2008).
[7]S. L. Means and M. Siderius, "Effects of sea-surface conditions on passive fathometry and bottom characterization," J. Acoust. Soc. Am. **126**, 2234–2241 (2009).
[8]P. Gerstoft, W. S. Hodgkiss, M. Siderius, C.-F. Huang, and C. H. Harrison, "Passive fathometer processing," J. Acoust. Soc. Am. **123**, 1297–1305 (2008).
[9]C. H. Harrison, "Anomalous signed passive fathometer impulse response when using adaptive beam forming," J. Acoust. Soc. Am. **125**, 3511–3513 (2009).
[10]J. Traer, P. Gerstoft, H. Song, and W. S. Hodgkiss, "On the sign of the adaptive passive fathometer impulse response," J. Acoust. Soc. Am. **126**, 1657–1658 (2009).
[11]A. Frantzis, "Does acoustic testing strand whales?," Nature (London) **392**, 29 (1998).
[12]J. Rickett and J. Claerbout, "Acoustic daylight imaging via spectral factorization: Helioseismology and reservoir monitoring," The Leading Edge **18**, 957–960 (1999).
[13]R. L. Weaver and O. I. Lobkis, "Ultrasonics without a source: Thermal

fluctuation correlations at MHz frequencies," Phys. Rev. Lett. **87**, 134301–134304 (2001).
[14]O. I. Lobkis and R. L. Weaver, "On the emergence of the Green's function in the correlations of a diffuse field," J. Acoust. Soc. Am. **110**, 3011–3017 (2001).
[15]P. Roux, W. A. Kuperman, and the NPAL Group, "Extracting coherent wave fronts from acoustic ambient noise in the ocean," J. Acoust. Soc. Am. **116**, 1995–2003 (2004).
[16]P. Roux, K. G. Sabra, and W. A. Kuperman, "Ambient noise cross correlation in free space: Theoretical approach," J. Acoust. Soc. Am. **117**, 79–83 (2005).
[17]L. A. Brooks and P. Gerstoft, "Green's function approximation from cross-correlations of 20–100 Hz noise during a tropical storm," J. Acoust. Soc. Am. **125**, 723–734 (2009).
[18]K. G. Sabra, P. Roux, and W. A. Kuperman, "Arrival-time structure of the time-averaged ambient noise cross-correlation function in an oceanic waveguide," J. Acoust. Soc. Am. **117**, 164–174 (2005).
[19]K. G. Sabra, P. Roux, and W. A. Kuperman, "Emergence rate of the time-domain Green's function from the ambient noise cross-correlation function," J. Acoust. Soc. Am. **118**, 3524–3530 (2005).
[20]O. A. Godin, "Recovering the acoustic Green's function from ambient noise cross correlation in an inhomogeneous moving medium," Phys. Rev. Lett. **97**, 054301 (2006).
[21]M. Siderius, P. L. Nielsen, and P. Gerstoft, "Range-dependent seabed characterization by inversion of acoustic data from a towed receiver array," J. Acoust. Soc. Am. **112**, 1523–1535 (2002).
[22]H. L. Van Trees, *Detection, Estimation, and Modulation Theory: Part IV: Optimum Array Processing* (Wiley, New York, 2002).
[23]W. S. Burdic, *Underwater Acoustic System Analysis* (Prentice-Hall, Englewood Cliffs, NJ, 1984).
[24]H. C. Song, W. A. Kuperman, W. S. Hodgkiss, P. Gerstoft, and J. S. Kim, "Null broadening with snapshot-deficient covariance matrices in passive sonar," IEEE J. Ocean. Eng. **28**, 250–261 (2003).
[25]H. Cox, R. M. Zeskind, and M. M. Owen, "Robust adaptive beamforming," IEEE Trans. Acoust., Speech, Signal Process. **35**, 1365–1376 (1987).
[26]C. W. Holland, "Coupled scattering and reflection measurements in shallow water," IEEE J. Ocean. Eng. **27**, 454–470 (2002).